Absolute Photoionization Cross-Section of the Methyl Radical†

Craig A. Taatjes,* David L. Osborn, Talitha M. Selby, and Giovanni Meloni

Combustion Research Facility, Mail Stop 9055, Sandia National Laboratories, Livermore, California 94551-0969

Haiyan Fan‡ and Stephen T. Pratt*

Argonne National Laboratory, Argonne, Illinois 60439

Received: March 16, 2008; Revised Manuscript Received: April 29, 2008

The absolute photoionization cross-section of the methyl radical has been measured using two completely independent methods. The CH_3 photoionization cross-section was determined relative to that of acetone and methyl vinyl ketone at photon energies of 10.2 and 11.0 eV by using a pulsed laser-photolysis/time-resolved synchrotron photoionization mass spectrometry method. The time-resolved depletion of the acetone or methyl vinyl ketone precursor and the production of methyl radicals following 193 nm photolysis are monitored simultaneously by using time-resolved synchrotron photoionization mass spectrometry. Comparison of the initial methyl signal with the decrease in precursor signal, in combination with previously measured absolute photoionization cross-sections of the precursors, yields the absolute photoionization cross-section of the methyl radical; $\sigma_{CH_3}(10.2\ \text{eV}) = (5.7 \pm 0.9) \times 10^{-18}$ cm^2 and $\sigma_{CH_3}(11.0\ \text{eV}) = (6.0 \pm 2.0) \times 10^{-18}$ cm^2. The photoionization cross-section for vinyl radical determined by photolysis of methyl vinyl ketone is in good agreement with previous measurements. The methyl radical photoionization cross-section was also independently measured relative to that of the iodine atom by comparison of ionization signals from CH_3 and I fragments following 266 nm photolysis of methyl iodide in a molecular-beam ion-imaging apparatus. These measurements gave a cross-section of $(5.4 \pm 2.0) \times 10^{-18}$ cm^2 at 10.460 eV, $(5.5 \pm 2.0) \times 10^{-18}$ cm^2 at 10.466 eV, and $(4.9 \pm 2.0) \times 10^{-18}$ cm^2 at 10.471 eV. The measurements allow relative photoionization efficiency spectra of methyl radical to be placed on an absolute scale and will facilitate quantitative measurements of methyl concentrations by photoionization mass spectrometry.

Introduction

The continuing implementation of synchrotron photoionization mass spectrometric measurements for investigations of chemically reacting systems such as low-pressure flames,[1–17] laser-initiated chemical kinetics[18–20] and aerosol chemistry[21] has led to a renewed interest in measurements of absolute photoionization cross-sections. Absolute cross-sections for photoionization are necessary to convert observed photoionization signals to mole fractions in molecular beam mass spectrometry investigations of low pressure flames, and to quantify branching fractions in elementary chemical kinetics measurements. Measurement of cross-sections for stable species has been carried out by a number of methods. Typically, the primary measurements of photoionization cross-sections are decomposed into a measurement of the absolute absorption cross-section and a determination of the ionization yield (i.e., the probability that absorption of a photon results in ionization). Dyke and coworkers[22] have measured absolute photoionization cross-sections of reactants and intermediates in the Cl_2 + dimethyl sulfide reaction by comparing photoelectron spectra of the species to reference photoelectron spectra of Ar under the same conditions. Person and Nicole[23–25] measured absolute cross-sections for absorption of isotopomers of several hydrocarbons and determined the ionization yield relative to that of NO, using the NO photoionization yield measurements of Watanabe et al.[26] to place the ionization cross-sections on an absolute scale. Recently, Cool and coworkers[1,10,27] have measured photoionization cross-sections of many stable combustion intermediates relative to hydrocarbon molecules whose absolute photoionization cross-sections are known from those earlier experiments. However, understanding the detailed chemistry of flames or of any reacting system requires knowledge of the radical species concentrations, and photoionization cross-sections of radicals are far less well-known.

One difficulty with many techniques to determine absolute photoionization cross-sections is the determination of the absolute concentration of radicals. One way to circumvent this issue is to use photodissociation of a suitable precursor to produce the desired radical in conjunction with a species of known cross-section. For example, Flesch et al.[28,29] have determined the absolute photoionization cross-section of ClO by photodissociating ClO_2 and Cl_2O, and making use of the known absolute photoionization cross-sections of O and Cl. More recently, Neumark and coworkers[30–32] have developed a related, but more general, approach that is applicable to larger radicals. This approach is based on translational spectroscopy and the photoionization of momentum-matched fragments produced by photodissociation. By using radical-chloride precursors, the known absolute photoionization cross-section of Cl could be used to extract the absolute cross-section of the radical. This novel approach has been successfully applied to allyl,[31]

† Part of the "Stephen R. Leone Festschrift".

* Authors to whom correspondence should be addressed. E-mail: cataatj@sandia.gov (C.A.T.); stpratt@anl.gov (S.T.P.).

‡ Current address: Department of Chemistry, Concordia College, 901 8th Street South, Moorhead, MN 56562.

10.1021/jp8022937 CCC: $40.75
Published on Web 06/21/2008

2-propenyl,[31] vinyl,[30] propargyl,[30] and phenyl[32] radicals and represents a significant advance in the determination of radical cross-sections. FitzPatrick et al.[33] have recently adopted this technique and applied it to the determination of the absolute photoionization cross-section of the ethyl radical.

The methyl radical is a species of great importance both in tropospheric chemistry and in combustion. As the simplest alkyl radical, it plays a central role in hydrocarbon flames and is a prominent intermediate in the atmospheric oxidation of many organic species. Methyl radicals have been detected by photoionization in molecular beam mass spectrometry investigations of low pressure flames[4,8,13,34] and in elementary chemical kinetics experiments,[18,35–40] but the photoionization cross-section of this important radical has until now not been measured. In the current study, two new approaches for the determination of absolute photoionization cross-sections of radicals are presented and applied to the methyl radical. Both techniques rely on the generation or depletion of a species of known photoionization cross-section in a concentration that is in a quantitative relationship to the concentration of the radical being measured. A relative ionization efficiency measurement can therefore be converted to an absolute ionization cross-section by applying the known concentration relationship and the known cross-section of the reference species. The first approach uses photolysis of a precursor of known photoionization cross-section to produce the radical of interest. If the branching fraction for dissociation into the desired product channel is known, then the concentration of the radical produced has a defined relationship to the depletion in concentration of the photolyte. The experiments are carried out in a slow-flow chemical reactor that is coupled to a dual-sector mass spectrometer, employing tunable synchrotron radiation for ionization.[18–20] The depletion of the precursor and the appearance of the radical product are monitored simultaneously on a time- and position-sensitive detector.

The second approach is closely related to that of Neumark and coworkers,[30–32] but the translational spectroscopy apparatus has been replaced by an ion-imaging apparatus, and the synchrotron vacuum-ultraviolet (VUV) light source has been replaced by a laser-based VUV source. The current approach has its roots in the ion-imaging work of Gross et al.[41] on the internal energy dependence of radical cross-sections. The ion-imaging approach results in a considerable simplification of the experiment, and the improved resolution of the translational energy distributions provides information on the internal state dependence of the radical cross-sections. The laser-based VUV source has the advantage of considerably higher resolution than the synchrotron-based source, and the disadvantages of being more difficult to tune over large energy regions and to calibrate with respect to photon flux.

Experiment

Synchrotron Photoionization Measurements. The chemical kinetic reactor apparatus will be described in greater detail elsewhere,[42] but the salient points are described here. It consists of a 60 cm long quartz slow-flow reactor,[43] in which reactions are photolytically initiated, coupled to a multiplexed photoionization mass spectrometer. Mass flow controllers deliver the photolytic precursor to the reactor in a large excess of helium. The beam of an unfocused, 4 Hz repetition rate excimer laser (193.3 nm) propagates down the tube, with a fluence of between 10 and 25 mJ cm^{-2} $pulse^{-1}$. A uniform density of CH_3 radicals is thereby created along the length of the tube. Gas is sampled continuously from the flow tube through a 650 μm diameter pinhole in the side of the tube. The nearly effusive beam emerging from the pinhole is skimmed before entering a differentially-pumped ionization region.

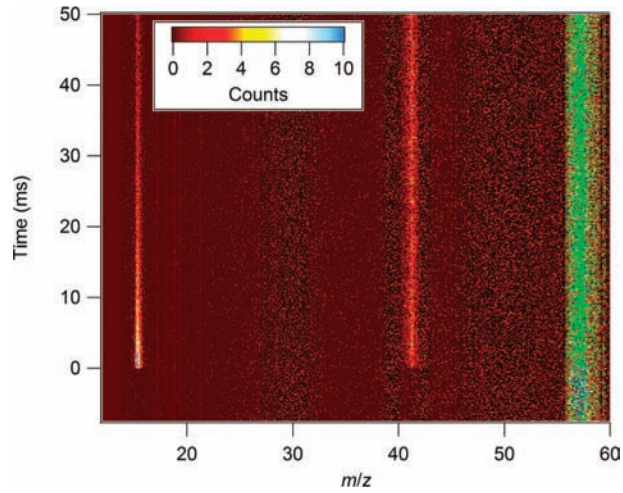

Figure 1. Time-resolved mass spectrum from photolysis of acetone at 193 nm taken at a photon energy of 10.2 eV. The mean signals from times before the photolysis pulse have been subtracted from the spectrum. The color scale covers positive values; pixels with a negative resultant, i.e., from photolytic depletion, are shown as green. The signal at $m/z = 42$ arises from the minor (~2%)[47] photodissociation channel that produces ketene (CH_2CO).

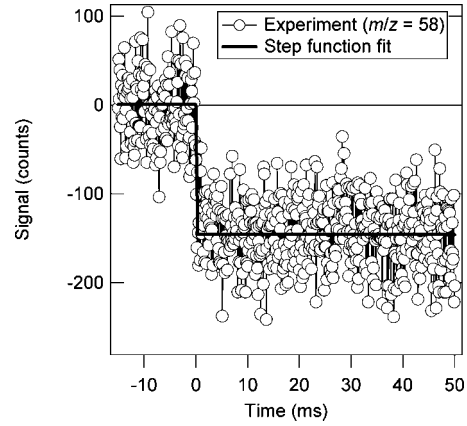

Figure 2. Depletion of the $m/z = 58$ signal from the dissociation of acetone, taken at a photon energy of 10.2 eV and binned with 100 μs time bins. The fit to a step function gives the depletion signal of (152 ± 6) counts.

The beam of sampled molecules is crossed in the ionization region by tunable synchrotron radiation from a 3 m monochromator at the Chemical Dynamics Beamline of the Advanced Light Source at Lawrence Berkeley National Laboratory. An Ar gas filter is placed in the beamline to suppress undulator harmonics at higher energy. The photon energy is calibrated by measurement of known atomic resonances of Xe, absorption resonances of Ar (using the gas filter as an absorption cell), and narrow autoionization resonances in O_2. Further confirmation of the energy calibration is made by measurement of the ionization threshold of acetone.[44] The light from the synchrotron ionizes molecules from the reactor within the ionization region of a miniature double-focusing Mattauch−Herzog-type mass spectrometer.[45] At the exit of the spectrometer, ions have been spatially dispersed according to their mass-to-charge ratio, and individual ions within a variable mass range of approximately 7 × (e.g., $m/z = 12$ to $m/z = 84$) are detected by a time- and position-sensitive microchannel plate detector with a delay-line

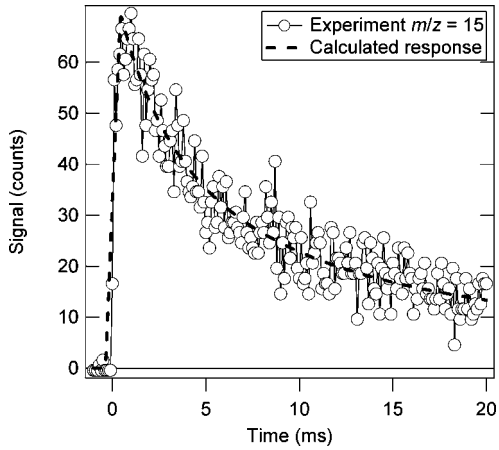

Figure 3. Time-resolved signal at $m/z = 15$ from dissociation of acetone, measured at a photon energy of 10.2 eV and binned with 100 μs time bins. A fit of a combined first- and second-order kinetic decay to the signal yields k', the product of the initial concentration and the effective second-order decay rate coefficient, of (130 ± 16) s^{-1}. The dashed line is the predicted signal for an initial ideal count level of 76 counts/bin and a k' of 130 s^{-1}, convolved with a theoretical instrument response function[51] calculated on the basis of a 298 K Maxwell−Boltzmann speed distribution and the 2.4 cm distance from the pinhole to the ionization region.

anode.[46] The position (which gives the mass) and time of arrival with respect to the photodissociation laser (with an inherent time resolution of 50 ns) are recorded simultaneously for each ion detected. The experiment is repeated, and the signal accumulated, for multiple laser pulses. As the native time and position resolution are fine enough that most pixels would have zero ions in a typical experiment, the accumulated counts are rebinned at lower resolution (e.g., 250 μs time bins) for analysis. The raw data retains the full time resolution, so a single set of data can be analyzed at several different choices of temporal and spatial bin sizes.

Figure 1 shows a section of the time-resolved mass spectrum taken for photodissociation of acetone at 193 nm. The average pre-photolysis signal is subtracted for each mass bin, yielding a differential signal proportional to the change in concentration upon photolysis. The observed negative-going signal at $m/z = 58$, $S_{58,t}$, as shown in Figure 2, is proportional to the dissociated acetone concentration $\Delta[\text{acetone}]_t$:

$$S_{58,t} = \alpha_{58}\sigma_{\text{acetone},58}\Delta[\text{acetone}]_t \quad (1)$$

where α_{58} is the instrument response for ions of $m/z = 58$ and $\sigma_{\text{acetone},58}$ is the partial photoionization cross-section for forming $m/z = 58$ ions from acetone. The observed signal at $m/z = 15$ (Figure 3) is proportional to the methyl radical concentration:

$$S_{15,t} = \alpha_{15}\sigma_{\text{methyl}}[\text{methyl}]_t \quad (2)$$

with corresponding instrument response function and photoionization cross-section. The methyl concentration and the change in acetone concentration are related immediately after the photolysis by the known dissociation yield,[47]

$$\frac{[\text{methyl}]_0}{\Delta[\text{acetone}]_0} = 1.91 \quad (3)$$

Dividing (2) by (1) yields the ratio of the initial signals:

$$\frac{S_{15,t\to 0}}{S_{58,t\to 0}} = 1.91\frac{\alpha_{15}\sigma_{\text{methyl},15}}{\alpha_{58}\sigma_{\text{acetone},58}} \quad (4)$$

The relative response function, α_{15}/α_{58}, is measured by taking the mass spectrum of a calibration mixture containing known mole fractions of several species with known photoionization cross-sections. The mass-dependent response is given to a good approximation by the square root of the masses (as found for similar mass sampling configurations),[48] so $\alpha_{15}/\alpha_{58} \approx (15/58)^{1/2} = 0.509$. Equation 4 can thus be rearranged to give the cross-section ratio in terms of the signal ratio:

$$\frac{\sigma_{\text{methyl},15}}{\sigma_{\text{acetone},58}} \approx 1.03\frac{S_{15,t\to 0}}{S_{58,t\to 0}} \quad (5)$$

The determinations using methyl vinyl ketone are carried out in a similar fashion, except that the parent molecule is at $m/z = 70$ and the dissociation yield for methyl vinyl ketone is taken as[49]

$$\frac{[\text{methyl}]_0}{\Delta[\text{methyl vinyl ketone}]_0} = (0.9 \pm 0.1) \quad (6)$$

(see below), and therefore the relationship between signals and cross-sections is

$$\frac{\sigma_{\text{methyl},15}}{\sigma_{\text{methyl vinyl ketone},70}} \approx 2.4\frac{S_{15,t\to 0}}{S_{70,t\to 0}} \quad (7)$$

The relative photoionization cross-sections can hence be obtained from extrapolation back to the initial ion signals.

Extraction of the initial acetone or methyl vinyl ketone depletion signal is straightforward, because the time profile for the precursor depletion is simply a step function, as seen in Figure 2. However, the methyl radical concentration decays on a timescale of several milliseconds, and the convolution with the time response function of the sampling[50,51] plays a significant role in the shape of the observed signal. To determine the signal level corresponding to the initial methyl concentration, the observed decay is first fit to the functional form of a combined first- and second-order decay. Extrapolation of this trace back to the zero of time gives an estimate of the initial methyl signal. However, this extrapolation can be rather sensitive to choice of the zero of time for the detected signal. Because the instrumental time response is affected by both the velocity spread in the beam and by the delay between molecules' exit from the reactor and their arrival at the ionization region, time zero is sometimes estimated as the half-way point of a detector-limited rise ("half-rise time").

In the present case, the fitted kinetic functions are explicitly convolved with an approximate response function[50,51] appropriate for the sampling geometry (an effusive expansion is used as an approximation to the present experiments, which are intermediate between effusive and supersonic sampling). This yields a profile corresponding to the ideal signal shape for the fitted kinetics and the known detection time response, with an unambiguous zero of time at the instant of the photolysis laser pulse. The dashed line in Figure 3 shows such a profile additionally convolved at the time binning used (100 μs bins for the data in Figure 3). The scaling of this profile to that calculated for a step function concentration change relates the fitted signal levels to those that would be observed for the initial radical concentration. Depending on the size of the time bins and the decay time constants, the initial signals extracted in this more rigorous way can differ by up to 20% from those derived from simple extrapolation of the fit to the half-rise time. Relative signals for each experiment are determined at several different time binnings to ensure that the determination is independent of the choice of time bin.

Ion-Imaging Measurements. The ion-imaging apparatus has been described in detail previously,[52–54] and is discussed only

briefly here. Indeed, the experimental approach is essentially identical to that described in ref 54, except for the replacement of the fixed 118 nm VUV source with a tunable four-wave mixing source. The apparatus consists of a pulsed, skimmed molecular beam source, standard collinear velocity map imaging ion optics, a channelplate detector coupled to a phosphor screen, and a video camera interfaced to a computer for data acquisition. In the present experiments, the molecular beam was crossed at right angles by the 266 nm output of a frequency-quadrupled Nd:YAG laser to photodissociate the sample, and the fragments were probed by using counter-propagating VUV light generated by two-photon resonant, four-wave mixing in Kr. All of the laser pulses were ~10 ns in duration.

The VUV light was generated in a small cell containing Kr, which was separated from the main chamber by a MgF_2 lens. The 202.315 nm light from a frequency-tripled, Nd:YAG-pumped dye laser was used to pump the two-photon Kr $^1S_0 \rightarrow 5p'[1/2]_0$ transition,[55] and the 675−695 nm light from a second Nd:YAG pumped dye laser was used to generate the difference frequency light around 10.46 eV. The laser wavelengths were calibrated by using a commercial wavemeter (Coherent Wavemaster). The two beams were focused into the Kr cell by using a 125 mm achromatic lens, and the diverging VUV light produced was refocused by the MgF_2 lens into the molecular beam. The chromatic aberration of the MgF_2 lens results in the generating beams being refocused well past the interaction region, and by aligning the lens slightly off center, the VUV light is effectively separated from the generating beams. The sample consisted of ~5% CH_3I in He at a backing pressure behind the pulsed valve of ~1200 Torr. The timing of the laser pulses was arranged to probe the initial rise of the gas pulse to minimize the presence of dimers and larger methyl iodide clusters in the beam. Typically, the 266 nm pulse arrived ~50 ns before the VUV pulse, and the signals from the two individual beams alone were characterized by blocking one or the other.

The absolute cross-section determinations require two separate measurements: recording the images of CH_3^+ and I^+ produced by single-photon ionization of the neutral CH_3 and I photofragments, and recording the relative intensities of the ion signals at the CH_3^+ and I^+ masses under the same condition as the images. The CH_3^+ and I^+ images were recorded as in previous experiments by gating the channelplate detector voltages on the mass of interest. For these measurements, images were averaged over 20000 to 60000 laser shots, and the images were reconstructed by using the BASEX program of Dribinski et al.[56] Integrating the reconstructed distributions over all angles yields the total translational energy distributions. These distributions were calibrated by using the known energetics of the dissociation process and previous measurements of the CH_3 vibrational distributions and I spin−orbit branching fractions.[57–60] The mass spectra were recorded by monitoring the time-of-flight ion signal on the detector anode and averaging over 400 laser shots. Mass spectra were also recorded with each of the laser beams blocked in turn, allowing background subtraction to isolate the true ion signal of interest from background produced by one or two of these beams alone.

These molecular-beam photolysis measurements do not exhibit the square-root dependence of the gas-dynamic sampling efficiency on mass that occurs in the flow reactor experiments. However, in these experiments the channelplates are operated in analog mode, unlike the discrete event-counting detection used in the flow reactor measurements, so here the signal must be corrected for the mass dependence of the channelplate gain. In particular, for a given acceleration or ion-impact energy, lighter ions result in higher gain than heavier ones. Oberheide et al.[61] have studied this dependence for the singly charged rare gas ions Ne^+, Ar^+, Kr^+, and Xe^+, as well as for H_2^+ and found a smooth behavior as a function of mass that is well described by the relations derived by Parilis and Kishinevskii.[62] Extrapolating their results to the present ions indicates that the channelplate gain for CH_3^+ is 1.52 times higher than that of I^+ at the acceleration voltages of our work. More recent studies by Krems et al.[63] have characterized the absolute ion detection efficiencies as a function of mass and impact energy for a dual channelplate detector of the present design and manufacturer. Under the present conditions, their results yield a CH_3^+ detection efficiency that is 1.46 times higher than that of I^+. The similarity of these values provides some confidence in the necessity and magnitude of this correction, and in what follows we use the average value for the correction of 1.49.

In principle, the magnitude of this correction and the uncertainty it introduces could be reduced considerably by using CH_3Cl as a precursor, so that the two ions to be compared would have more similar masses. Indeed, chlorinated precursors were used in the work of Neumark and coworkers.[30–32] Unfortunately, the ionization energy of Cl (13.017 eV)[64] is considerably higher than that of I (10.451 eV),[55] and requires windowless operation of the VUV cell. Obtaining the CH_3 cross-section above 13.0 eV may also be complicated by dissociative ionization, while measuring the CH_3 cross-section at 10.46 eV relative to the Cl cross-section above 13.017 eV would require an accurate knowledge of the VUV flux in the interaction region at the two energies. While modifications to the apparatus to accommodate such measurements are underway, it remains to be seen how precise such measurements can be made. The advantage of using CH_3I is that both fragments can be measured at the same photon energy, obviating the need for VUV flux measurements.

Berkowitz et al.[65] have determined the relative photoionization cross-section of I ($^2P_{3/2}$) between threshold and ~14 eV, but to our knowledge there have been no experimental determinations of the absolute photoionization cross-section in this region. However, Robicheaux and Greene[66] have calculated the absolute photoionization cross-section of I ($^2P_{3/2}$) throughout this region, along with the corresponding cross-sections of the other halogens, by using a combination of R-matrix methods and multichannel quantum defect theory. The agreement between these calculations and the experimental absolute photoionization cross-sections is quite good for F, Cl, and Br. The calculations on I are expected to be the most difficult, but although the resonance positions are not reproduced precisely, the overall appearance and major features are well reproduced.

For the present determination, the I ($^2P_{3/2}$) cross-section is required at three energies just above the I^+ ($^3P_2$) threshold. The spectrum of Berkowitz et al.[65] shows that these energies lie on the high energy edge of a very intense ($^3P_0$)5s autoionizing resonance and somewhat below an intense ($^3P_1$)5s resonance. The positions of these resonances are somewhat shifted in the calculation of Robicheaux and Greene.[66] Thus, we have extracted the required absolute cross-sections by interpolating the positions between the two resonances in the spectrum of Berkowitz et al.,[65] and used the cross-sections of Robicheaux and Greene[66] at the same positions relative to the theoretical energies. The absolute cross-sections so obtained are 170×10^{-18} cm^2 at 10.461 eV, 130×10^{-18} cm^2 at 10.466 eV, and 110×10^{-18} cm^2 at 10.471 eV. We note that the length and velocity gauge calculations are in good agreement, and that although the theoretical spectra were convolved with the experimental resolution for comparison with the data of

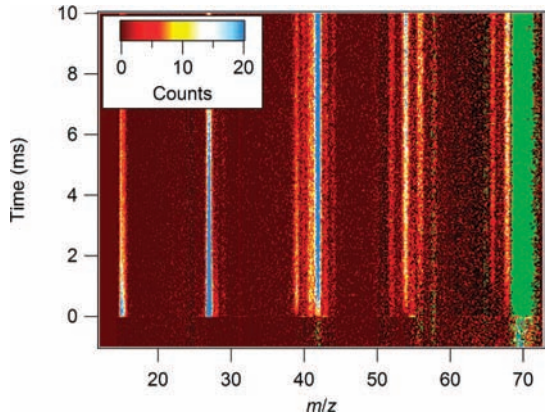

Figure 4. Time-resolved mass spectrum from photolysis of methyl vinyl ketone at 193 nm taken at a photon energy of 10.2 eV. The mean signals from times before the photolysis pulse have been subtracted from the spectrum. Pixels with a negative resultant (i.e., from photolytic depletion) are shown as green (not given on the color scale).

Berkowitz et al.,[65] the widths of the relevant resonances are considerably greater than the experimental resolution.

Although the error bars for the I ($^2P_{3/2}$) absolute cross-sections are somewhat difficult to assess, the potential for future improvements is clear. On the theoretical side, larger scale calculations are certainly possible given the increase in computational power since 1992. On the experimental side, a windowless VUV source would allow the determination of the I ($^2P_{3/2}$) cross-section relative to the more precisely known Cl ($^2P_{3/2}$) and Br ($^2P_{3/2}$) cross-sections by using the photodissociation of ICl or IBr. Together, such improvements are expected to enhance the accuracy of the approach for the determination of absolute photoionization cross-sections of radicals.

Results and Discussion

Synchrotron Photoionization Measurements. The relative cross-section measurements for methyl and acetone at 10.2 and 11.0 eV can be placed on an absolute scale by comparison with the absolute partial photoionization cross-sections for acetone reported by Cool et al.[27] under similar conditions, using eq 5. This evaluation gives photoionization cross-sections for the methyl radical of $(5.9 \pm 1.4) \times 10^{-18}$ cm^2 at 10.2 eV photon energy and $(6.0 \pm 1.8) \times 10^{-18}$ cm^2 at 11.0 eV. The reported ($\pm 2\sigma$) uncertainty limits include the combined uncertainty of approximately 10−15% in the fits to the data, scatter of the repeated determinations, and estimated uncertainties in the mass dependence of the signal response α and in the literature cross-section of acetone.

The yield of methyl radicals in the photolysis of methyl vinyl ketone has been less extensively investigated than that of acetone. The principal product channel of methyl vinyl ketone photolysis was determined by Fahr et al.[49] to be methyl + vinyl + CO, with a dissociation yield near unity. An experimental dissociation yield can be computed by dividing their derived methyl concentrations (given as percentages of initial methyl vinyl ketone) by their measured methyl vinyl ketone depletion, reported as (23.6 ± 1.1) %.[49] Using the methyl yield determined from gas chromatographic analysis of the stable products[49] gives (0.88 ± 0.11), and using that derived from modeling 216.4 nm absorption data[49] gives (0.95 ± 0.14). Stoliarov, Knyazev, and Slagle[40] observed minor signals at $m/z = 14$, $m/z = 43$, and $m/z = 54$ that they attributed to photolysis of methyl vinyl ketone, but confirmed the dominance of the channel forming $CH_3 + C_2H_3 + CO$. Figure 4 shows a section of a time-resolved mass spectrum taken at 10.2 eV ionization energy for the 193 nm photolysis of methyl vinyl ketone. The dominant peaks arise from the formation of CH_3 ($m/z = 15$) + C_2H_3 ($m/z = 27$) + CO and their subsequent reactions. For example, the vinyl + vinyl reaction forms 1,3-butadiene ($m/z = 54$) and propargyl ($m/z = 39$) + methyl, and the methyl + vinyl reaction forms propene ($m/z = 42$). However, components of the signals at $m/z = 55$, $m/z = 43$, and possibly $m/z = 29$ and $m/z = 41$ are formed promptly with the laser pulse and can likely be attributed to direct photolysis products. These signals are relatively small, but their existence implies a yield of the $CH_3 + C_2H_3 + CO$ that is smaller than unity. Although a detailed analysis of the photodissociation process is beyond the scope of this work, if a typical photoionization cross-section of 10 Mb[27] is assumed for all the prompt species, the observed signals are roughly consistent with 5−10% of the photodissociation proceeding by channels other than $CH_3 + C_2H_3 + CO$. For the purposes of the cross-section measurements, a yield of (0.9 ± 0.1) has therefore been used.

Absolute partial photoionization cross-sections for methyl vinyl ketone have been measured by Wang et al.;[67] at 10.2 eV the cross-section for production of parent ($m/z = 70$) ion is 10.7×10^{-18} cm^2, with an uncertainty ($\pm 2\sigma$) likely to be approximately 15%, as in other photoionization cross-section measurements by the same group.[10] Using the measured relative ionization signals of methyl and methyl vinyl ketone from three determinations at 10.2 eV with this cross-section and a methyl yield of (0.9 ± 0.1) results in a methyl cross-section determination of $(5.6 \pm 1.1) \times 10^{-18}$ cm^2, where the reported total uncertainty includes propagated uncertainties in the photodissociation yield, the fits to the data, and the methyl vinyl ketone cross-section. A similar procedure applied to the vinyl radical signals yields a photoionization cross-section for vinyl radical of $(10 \pm 2) \times 10^{-18}$ cm^2, in good agreement with the determination of Robinson, Sveum, and Neumark,[30] who measured the cross-section relative to that of Cl atom. The average of the acetone and methyl vinyl ketone determinations gives the final measured value of $(5.7 \pm 0.9) \times 10^{-18}$ cm^2 for the methyl radical photoionization cross-section at 10.2 eV.

Ion-Imaging Measurements. As discussed above, the concept idea behind these measurements is essentially identical to that of the experiments of Neumark and coworkers,[30−32] that is, that the photodissociation of CH_3I produces one CH_3 radical for every I atom. If both photofragments are produced in a single quantum state, and the absolute photoionization cross-section of the I atom is known, the comparison of the total ion signals at the CH_3^+ and I^+ masses at a given VUV photon energy would provide the absolute photoionization cross-section of CH_3. Unfortunately, the photodissociation process not only produces CH_3 in a distribution of vibrational and rotational states, it also produces I atoms in both the $^2P_{3/2}$ ground state and $^2P_{1/2}$ spin−orbit excited state.[58−60] However, reconstruction of the CH_3^+ and I^+ ion images allows a determination of the translational energy distributions for the two fragments and thus allows the partitioning of the total ion signal at the two masses into the different product channels.

As illustration, Figure 5 shows the CH_3^+ and I^+ images obtained following the 266 nm photodissociation of CH_3I and using single-photon VUV ionization at 10.466 eV, and Figure 6 shows the corresponding translational energy distributions obtained by reconstructing the two images. By comparing the intensities of the CH_3^+ and I^+ ion signals in each channel, that is, by comparing the ion signal from momentum-matched fragments, the absolute photoionization cross-sections for CH_3

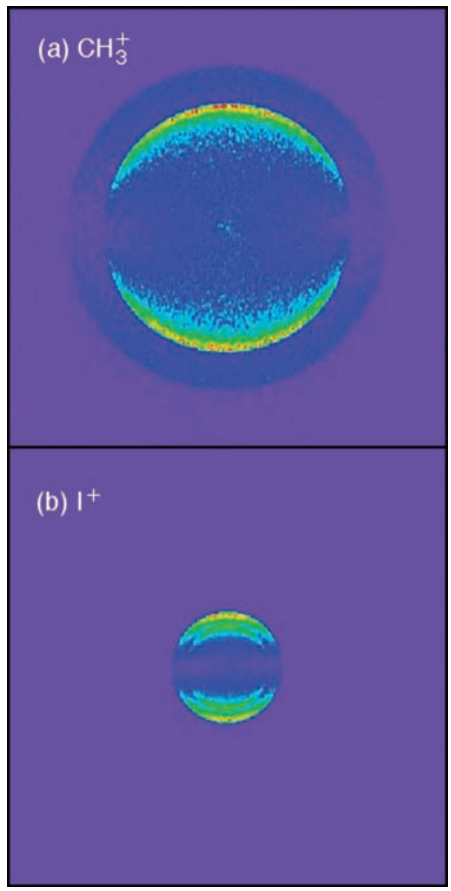

Figure 5. Velocity map ion images produced following the 266 nm photodissociation of CH_3I and ionizing the fragments by using a single photon at 10.466 eV: (a) CH_3^+ image; (b) I^+ image.

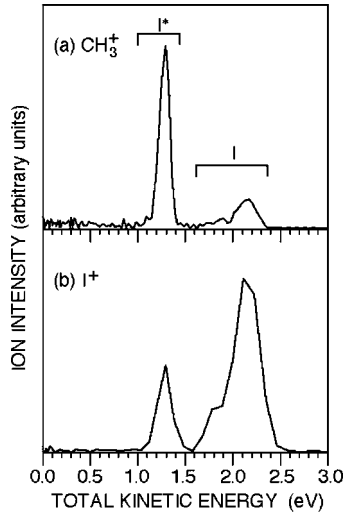

Figure 6. Total translational energy distributions obtained from the reconstruction of the ion images shown in Figure 1: (a) from the CH_3^+ image; (b) from the I^+ image.

can be extracted if the I ($^2P_{3/2}$) cross-section is known. In addition, to the extent that the vibrational (or rotational) levels of CH_3 are resolved in the translational energy distributions, these cross-sections can be determined as a function of vibrational (or rotational) level. The key to this determination is that in the I^+ image and translational energy distributions, the $^2P_{3/2}$ and $^2P_{1/2}$ channels are fully resolved, and that within the $^2P_{3/2}$ channel (or $^2P_{1/2}$ channel), the relative intensities give the true branching fractions because it is always $^2P_{3/2}$ atoms (or $^2P_{1/2}$ atoms) that are being ionized. In contrast, the relative intensities in the CH_3 image and translational energy distribution are determined by the product of the true branching fraction and the relative photoionization cross-section of the relevant vibrational level. Note, however, that even in the I^+ image, the relative intensities of the integrated I ($^2P_{3/2}$) and I ($^2P_{1/2}$) channels do not reflect the true spin−orbit branching fractions, as these are weighted by the photoionization cross-sections of I ($^2P_{3/2}$) or I ($^2P_{1/2}$), respectively, and these are not necessarily the same at the VUV energy of interest. However, because the I ($^2P_{3/2}$) and I ($^2P_{1/2}$) branching fractions following the 266 nm photodissociation of CH_3I are known, they can be used with the I ($^2P_{3/2}$) absolute photoionization cross-section to determine the absolute $^2P_{1/2}$ cross-section. The I ($^2P_{1/2}$) cross-section is now discussed, followed by the vibrational dependence of the CH_3 photoionization cross-section. As discussed previously, the latter dependence is quite weak at the VUV energies of the present study. Finally, the ion-imaging determination of the absolute photoionization cross-section of CH_3 is presented.

The photodissociation of CH_3I at 266 nm has been studied previously in great detail,[58–60] and the $^2P_{3/2}$ and $^2P_{1/2}$ branching fractions are 0.27 ± 0.04 and 0.73 ± 0.04, respectively. Simple inspection of Figure 6a reveals a very different ratio of intensities in the two channels, suggesting very different photoionization cross-sections at this VUV energy. As discussed above, for I ($^2P_{3/2}$) atoms, the VUV photon energies are very close to the peak of an intense autoionizing resonance, which strongly enhances the signal in this channel. Although no photoionization spectrum of I ($^2P_{1/2}$) has been reported previously, adding the spin−orbit energy[55] of 0.943 eV to the photon energy yields a total energy of ~11.41 eV. In the $^2P_{3/2}$ spectrum,[65] this energy corresponds to a region free from sharp resonances, and it is actually quite close to the minimum of a broad Beutler−Fano resonance. Single-photon selection rules indicate that any resonance allowed from the $^2P_{1/2}$ level will also be allowed from the $^2P_{3/2}$ level, so the former cross-section is also expected to be free from sharp resonances in the region of interest; it may even be close to a minimum.

The relative intensities of the I ($^2P_{3/2}$) and I ($^2P_{1/2}$) components in the translational energy distribution of Figure 6b are related to the branching fractions and absolute cross-sections by:

$$\frac{I_{rel}(^2P_{1/2})}{I_{rel}(^2P_{3/2})} = \frac{B(^2P_{1/2})}{B(^2P_{3/2})} \frac{\sigma(^2P_{1/2})}{\sigma(^2P_{3/2})} \quad (8)$$

where $I_{rel}(^2P_J)$ is the integrated intensity of the ^2P_J component in the translational energy distribution, $B(^2P_J)$ is the known branching fraction for the I (^2P_J) fine-structure state following 266 nm photodissociation of CH_3I, and $\sigma(^2P_J)$ is the absolute photoionization cross-section of the ^2P_J level at the VUV energy of interest. Given the $I_{rel}(^2P_J)$ and $B(^2P_J)$ values for both states and the $\sigma(^2P_{3/2})$, this approach yields $\sigma(^2P_{1/2}) = (16 \pm 2) \times 10^{-18}$ cm^2 at 10.460 eV, $(13 \pm 2) \times 10^{-18}$ cm^2 at 10.466 eV, and $(11 \pm 2) \times 10^{-18}$ cm^2 at 10.471 eV. These values are indeed relatively small and consistent with close proximity to a resonance minimum in the cross-section. For comparison, between 11.409 eV and 11.414 eV (the total energy accessed from the $^2P_{1/2}$ state relative to the ground state energy), the corresponding photoionization cross-section of I ($^2P_{3/2}$) falls from $\sim 45 \times 10^{-18}$ to $\sim 38 \times 10^{-18}$ cm^2.[65,66]

The translational energy distribution of Figure 6 shows partially resolved vibrational structure within both the I ($^2P_{3/2}$) and I ($^2P_{1/2}$) channels. This structure is somewhat better resolved in images obtained at lower acceleration voltages. Given the

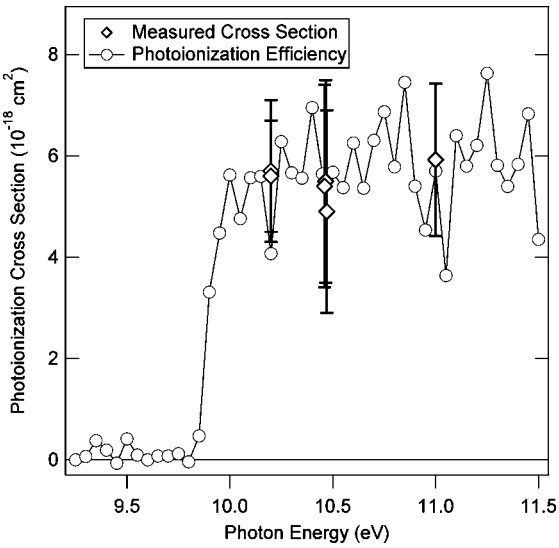

Figure 7. Low-resolution photoionization efficiency curve of the methyl radical (open circles), scaled by the present measurements of the photoionization cross-section (open lozenges). The esimated ($\pm 2\sigma$) uncertainty is shown as the error bars on the cross-section measurements.

known vibrational frequencies of CH_3, the intensities can be fit using Gaussian functions, with the integrated areas yielding the relative intensities of the different CH_3 vibrational bands in the two I fine-structure channels. The intensities of these bands are a product of the true vibrational branching fractions for the photodissociation process and the relative cross-sections for photoionization of these CH_3 vibrational levels at the energy of interest. These observed band intensities can be compared with the vibrational branching fractions for the two spin orbit channels determined by high resolution translational spectroscopy.[59] As discussed previously, the CH_3 photoionization cross-section appears to be essentially independent of the vibrational level at the photon energies of the present study. In particular, although measurements in the $^2P_{3/2}$ channel indicate the CH_3 (0,0,0,0) cross-section is slightly smaller than those of the CH_3 ($0,\upsilon_2>0,0,0$) levels, the measurements in the $^2P_{1/2}$ channel show the opposite behavior, indicating that the small variations are most likely the result of statistical fluctuations. Here ($\upsilon_1,\upsilon_2,\upsilon_3,\upsilon_4$) indicate the vibrational quantum numbers of the four vibrational modes of CH_3, and υ_2 corresponds to the umbrella motion of planar CH_3. The lack of vibrational dependence is not surprising because the CH_3 ground state highest occupied molecular orbital (HOMO) is non-bonding and the CH_3^+ ground state geometry is very similar to that of the neutral. As a result, the Franck−Condon envelopes for photoionization are expected to be very narrow, i.e., essentially delta functions for the $\Delta\upsilon_i = 0$ transitions. Because the VUV energies are ~0.8 eV above the vertical ionization threshold, no strong vibrational dependence is expected.

The lack of a strong vibrational dependence is confirmed by comparing the integrated intensities in the I ($^2P_{3/2}$) and I ($^2P_{1/2}$) components of the CH_3 translational energy distributions. These relative intensities yield I ($^2P_{3/2}$) and I ($^2P_{1/2}$) intensities of 0.28 and 0.72, respectively, i.e., essentially identical to the previously reported branching fractions of 0.27 ± 0.04 and 0.73 ± 0.04, respectively.[60] Because the CH_3 vibrational distributions are very different in the two spin−orbit channels, this observation also implies that the vibrational dependence of the CH_3 photoionization cross-section is weak at the present VUV energies. Thus, in what follows, this dependence is ignored, and the integrated intensities of the $^2P_{3/2}$ and $^2P_{1/2}$ band progressions are used.

The CH_3 rotational structure is completely unresolved in the present images. The rotational distributions produced by the photodissociation of CH_3I depend on both the CH_3 vibrational level and on the fine-structure level of the complementary I atoms. However, the photon energies of interest are sufficiently above threshold to span the full rotational envelopes, and in the absence of strong heterogeneous perturbations, the photoionization intensity integrated over the full rotational envelope is expected to be independent of the rotational temperature.[68]

Following these preliminaries, the actual cross-section determinations are straightforward. Independent sets of CH_3^+ and I^+ images and mass spectra were recorded at three VUV energies. The translational energy distributions from the reconstructed images provide the fractions of the CH_3^+ and I^+ ion signals in the I ($^2P_{3/2}$) channel [$F_{^2P_{3/2}}(CH_3^+)$ and $F_{^2P_{3/2}}(I^+)$, respectively]. Thus, the ratio of absolute cross-sections is given by

$$\frac{\sigma_{abs}^{CH_3}(\lambda)}{\sigma_{abs}^{I^2P_{3/2}}(\lambda)} = \left[\frac{F_{^2P_{3/2}}(CH_3^+)\, I_T(CH_3^+)}{F_{^2P_{3/2}}(I^+)\, I_T(I^+)}\right] D\left(\frac{I^+}{CH_3^+}\right) \qquad (9)$$

where the I_T are the total ion signals at the two masses and $D(I^+/CH_3^+)$ is the ratio of the detector gains for I^+ and CH_3^+ discussed above. Using the results of the measurements and the known $\sigma_{abs}^{I^2P_{3/2}}$ yields $\sigma_{abs}^{CH_3}(\lambda) = (5.4 \pm 2.0) \times 10^{-18}$ cm^2 at 10.460 eV, $(5.5 \pm 2.0) \times 10^{-18}$ cm^2 at 10.466 eV, and $(4.9 \pm 2.0) \times 10^{-18}$ cm^2 at 10.471 eV. The error bars reflect not only the measurement statistics but also the estimated uncertainty in the I ($^2P_{3/2}$) cross-section and the mass-dependent detector gain. As expected, the observed cross-sections are essentially constant over this small energy range. This consistency is particularly encouraging considering the large variation in the I ($^2P_{3/2}$) cross-section at these energies. The values are slightly smaller than those of the synchrotron measurements, but well within the error bars of either measurement.

The measurements of the cross-section at single photon energies can be used to place the relative photoionization efficiency of CH_3 on an absolute scale. Figure 7 shows a relatively low-resolution (60 meV) scan of the methyl photoionization spectrum, scaled by the present absolute measurements. In the absence of sharp resonances, the higher resolution spectra of, for example, Litorja and Ruscic[69] or Chupka and Lifshitz,[70] can also be scaled by the present measurements. The data of Litorja and Ruscic[69] do not extend above 10 eV, but the data of Chupka and Lifshitz,[70] recorded at a resolution of ~13 meV, extends to 11.5 eV. The latter work shows the CH_3 photoionization spectra from several runs and with different precursors. Taken together, there is evidence for some weak structure below ~10.25 eV that may be due to autoionizing resonances. Between 10.25 eV and 11.00 eV, however, the spectrum is relatively flat, and consistent with Figure 7.

Conclusion

The photoionization cross-section for the methyl radical has been determined by two independent methods. The determinations are in very good agreement and can be used to place the photoionization efficiency spectrum of CH_3 on an absolute scale. This measurement allows this key combustion and atmospheric chemistry intermediate to be measured quantitatively in photoionization mass spectrometry experiments. The two methods for the determination of absolute photoionization cross-sections presented here appear to be quite general, and should be applicable to a wide range of radicals and reactive species.

Acknowledgment. We thank Juan Wang and Terrill A. Cool (Cornell University) for providing their cross-section measurements of methyl vinyl ketone prior to publication. This work is supported by the Division of Chemical Sciences, Geosciences, and Biosciences, the Office of Basic Energy Sciences, the U.S. Department of Energy. The work at Argonne was supported by the U.S. Department of Energy, Office of Science, Office of Basic Energy Sciences, Division of Chemical Sciences, Geosciences, and Biosciences under contract No. DE-AC02-06CH11357. Sandia is a multiprogram laboratory operated by Sandia Corporation, a Lockheed Martin Co., for the National Nuclear Security Administration under contract DE-AC04-94-AL85000. The Advanced Light Source is supported by the Director, Office of Science, Office of Basic Energy Sciences, Materials Sciences Division, of the U.S. Department of Energy under Contract No. DE-AC02-05CH11231 at Lawrence Berkeley National Laboratory.

References and Notes

(1) Cool, T. A.; Nakajima, K.; Mostefaoui, T. A.; Qi, F.; McIlroy, A.; Westmoreland, P. R.; Law, M. E.; Poisson, L.; Peterka, D. S.; Ahmed, M. *J. Chem. Phys.* **2003**, *119*, 8356.

(2) Taatjes, C. A.; Osborn, D. L.; Cool, T. A.; Nakajima, K. *Chem. Phys. Lett.* **2004**, *394*, 19.

(3) Cool, T. A.; McIlroy, A.; Qi, F.; Westmoreland, P. R.; Poisson, L.; Peterka, D. S.; Ahmed, M. *Rev. Sci. Instrum.* **2005**, *76*, 094102.

(4) Cool, T. A.; Nakajima, K.; Taatjes, C. A.; McIlroy, A.; Westmoreland, P. R.; Law, M. E.; Morel, A. *Proc. Combust. Inst.* **2005**, *30*, 1681.

(5) Werner, J. H.; Cool, T. A. *Chem. Phys. Lett.* **1998**, *290*, 81.

(6) Taatjes, C. A.; Klippenstein, S. J.; Hansen, N.; Miller, J. A.; Cool, T. A.; Wang, J.; Law, M. E.; Westmoreland, P. R. *Phys. Chem. Chem. Phys.* **2005**, *7*, 806.

(7) Taatjes, C. A.; Hansen, N.; McIlroy, A.; Miller, J. A.; Senosiain, J. P.; Klippenstein, S. J.; Qi, F.; Sheng, L.; Zhang, Y.; Cool, T. A.; Wang, J.; Westmoreland, P. R.; Law, M. E.; Kasper, T.; Kohse-Höinghaus, K. *Science* **2005**, *308*, 1887.

(8) McIlroy, A.; Hain, T. D.; Michelsen, H. A.; Cool, T. A. *Proc. Combust. Inst.* **2000**, *28*, 1647.

(9) Taatjes, C. A.; Hansen, N.; Miller, J. A.; Cool, T. A.; Wang, J.; Westmoreland, P. R.; Law, M. E.; Kasper, T.; Kohse-Höinghaus, K. *J. Phys. Chem. A* **2006**, *110*, 3254.

(10) Wang, J.; Yang, B.; Cool, T. A.; Hansen, N.; Kasper, T. *Int. J. Mass Spectrom.* **2008**, *269*, 210.

(11) Oβwald, P.; Struckmeier, U.; Kasper, T.; Kohse-Höinghaus, K.; Wang, J.; Cool, T. A.; Hansen, N.; Westmoreland, P. R. *J. Phys. Chem. A* **2007**, *111*, 4093.

(12) Taatjes, C. A.; Hansen, N.; Osborn, D. L.; Kohse-Höinghaus, K.; Cool, T. A.; Westmoreland, P. R. *Phys. Chem. Chem. Phys.* **2008**, *10*, 20.

(13) Huang, C.; Wei, L.; Yang, B.; Wang, J.; Li, Y.; Sheng, L.; Zhang, Y.; Qi, F. *Energy Fuels* **2006**, *20*, 1505.

(14) Zhang, T.; Tang, X. N.; Lau, K.-C.; Ng, C. Y.; Nicolas, C.; Peterka, D. S.; Ahmed, M.; Morton, M. L.; Ruscic, B.; Yang, R.; Wei, L. X.; Huang, C. Q.; Yang, B.; Wang, J.; Sheng, L. S.; Zhang, Y. W.; Qi, F. *J. Chem. Phys.* **2006**, *124*, 074302.

(15) Yang, B.; Oβwald, P.; Li, Y.; Wang, J.; Wei, L.; Tian, Z.; Qi, F.; Kohse-Höinghaus, K. *Combust. Flame* **2007**, *148*, 198.

(16) Qi, F.; McIlroy, A. *Combust. Sci. Technol.* **2005**, *177*, 2021.

(17) Qi, F.; Yang, R.; Yang, B.; Huang, C. Q.; Wei, L. X.; Wang, J.; Sheng, L. S.; Zhang, Y. W. *Rev. Sci. Instrum.* **2006**, *77*, 084101.

(18) Meloni, G.; Zou, P.; Klippenstein, S. J.; Ahmed, M.; Leone, S. R.; Taatjes, C. A.; Osborn, D. L. *J. Am. Chem. Soc.* **2006**, *128*, 13559.

(19) Goulay, F.; Osborn, D. L.; Taatjes, C. A.; Zou, P.; Meloni, G.; Leone, S. R. *Phys. Chem. Chem. Phys.* **2007**, *9*, 4291.

(20) Meloni, G.; Selby, T. M.; Goulay, F.; Leone, S. R.; Osborn, D. L.; Taatjes, C. A. *J. Am. Chem. Soc.* **2007**, *129*, 14019.

(21) Mysak, E. R.; Wilson, K. R.; Jiminez-Cruz, M.; Ahmed, M.; Baer, T. *Anal. Chem.* **2005**, *77*, 5953.

(22) Dyke, J. M.; Ghosh, M. V.; Goubet, M.; Lee, E. P. F.; Levita, G.; Miqueu, K.; Shallcross, D. E. *Chem. Phys.* **2006**, *324*, 85.

(23) Person, J. C. *J. Chem. Phys.* **1965**, *43*, 2553.

(24) Person, J. C.; Nicole, P. P. *J. Chem. Phys.* **1968**, *49*, 5421.

(25) Person, J. C.; Nicole, P. P. *J. Chem. Phys.* **1970**, *53*, 1767.

(26) Watanabe, K.; Matsunaga, F. M.; Sakai, H. *Appl. Opt.* **1967**, *6*, 391.

(27) Cool, T. A.; Wang, J.; Nakajima, K.; Taatjes, C. A.; McIlroy, A. *Int. J. Mass. Spectrom.* **2005**, *247*, 18.

(28) Flesch, R.; Schürmann, M. C.; Plenge, J.; Hunnekuhl, M.; Meiss, H.; Bischof, M.; Rühl, E. *Phys. Chem. Chem. Phys.* **1999**, *1*, 5423.

(29) Flesch, R.; Plenge, J.; Kühl, S.; Klusmann, M.; Rühl, E. *J. Chem. Phys.* **2002**, *117*, 9663.

(30) Robinson, J. C.; Sveum, N. E.; Neumark, D. M. *J. Chem. Phys.* **2003**, *119*, 5311.

(31) Robinson, J. C.; Sveum, N. E.; Neumark, D. M. *Chem. Phys. Lett.* **2004**, *383*, 601.

(32) Sveum, N. E.; Goncher, S. J.; Neumark, D. M. *Phys. Chem. Chem. Phys.* **2005**, *8*, 592.

(33) FitzPatrick, B. L.; Maienschein-Cline, M.; Butler, L. J.; Lee, S.-H.; Lin, J. J. *J. Phys. Chem. A* **2007**, *111*, 12417.

(34) Hansen, N.; Miller, J. A.; Taatjes, C. A.; Wang, J.; Cool, T. A.; Law, M. E.; Westmoreland, P. R.; Kasper, T.; Kohse-Höinghaus, K. *Proc. Combust. Inst.* **2007**, *31*, 1157.

(35) Timonen, R. S.; Gutman, D. *J. Phys. Chem.* **1986**, *90*, 2987.

(36) Knyazev, V. D.; Slagle, I. R. *J. Phys. Chem. A* **1998**, *102*, 1770.

(37) Seetula, J. A.; Russell, J. J.; Gutman, D. *J. Am. Chem. Soc.* **1990**, *112*, 1347.

(38) Niiranen, J. T.; Gutman, D. *J. Phys. Chem.* **1993**, *97*, 9392.

(39) Knyazev, V. D.; Bencsura, A.; Stoliarov, S. I.; Slagle, I. R. *J. Phys. Chem.* **1996**, *100*, 11346.

(40) Stoliarov, S. I.; Knyazev, V. D.; Slagle, I. R. *J. Phys. Chem. A* **2000**, *104*, 9687.

(41) Gross, R. L.; Liu, X.; Suits, A. G. *Chem. Phys. Lett.* **2002**, *362*, 229.

(42) Osborn, D. L.; Zou, P.; Johnsen, H.; Hayden, C. C.; Taatjes, C. A.; Peterka, D. S.; Ahmed, M.; Leone, S. R. The *Multiplexed Chemical Kinetic Photoionization Mass Spectrometer: A New Approach for Isomer Resolved Chemical Kinetics*. In preparation.

(43) Slagle, I. R.; Gutman, D. *J. Am. Chem. Soc* **1985**, *107*, 5342.

(44) Trott, W. M.; Blais, N. C.; Walters, E. A. *J. Chem. Phys.* **1978**, *69*, 3150.

(45) Sinha, M. P.; Wadsworth, M. *Rev. Sci. Instrum.* **2005**, *76*, 025103.

(46) Vallerga, J. V.; Siegmund, O. H. W. *Nucl. Instrum. Methods Phys. Res. A* **2000**, *442*, 159.

(47) Lightfoot, P. D.; Kirwan, S. P.; Pilling, M. J. *J. Phys. Chem.* **1988**, *92*, 4938.

(48) Hsu, W. L.; Tung, D. M. *Rev. Sci. Instrum.* **1992**, *63*, 4138.

(49) Fahr, A.; Braun, W.; Laufer, A. H. *J. Phys. Chem.* **1993**, *97*, 1502.

(50) Moore, S. B.; Carr, R.W., Jr *Int. J. Mass Spectrom. Ion Phys.* **1977**, *24*, 161.

(51) Taatjes, C. A. *Int. J. Chem. Kinet.* **2007**, *39*, 565.

(52) Eppink, A. T. J. B.; Parker, D. H. *Rev. Sci. Instrum.* **1997**, *68*, 3477.

(53) Aguirre, F.; Pratt, S. T. *J. Chem. Phys.* **2002**, *118*, 1175.

(54) Aguirre, F.; Pratt, S. T. *J. Chem. Phys.* **2005**, *122*, 234303.

(55) Moore, C. E. *Atomic Energy Levels (Nat. Bur. Stand. Circular 467)*; Dept. of Commerce: Washington, D.C., 1952.

(56) Dribinski, V.; Ossadtchi, A.; Mandelshtam, V.; Reisler, H. *Rev. Sci. Instrum.* **2002**, *73*, 2634.

(57) *NIST Chemistry WebBook, NIST Standard Reference Database Number 69*; Linstrom, P. J.; Mallard, W. G. Eds.; National Institute of Standards and Technology: Gaithersburg, MD, 2003.

(58) Eppink, A. T. J. B.; Parker, D. H. *J. Chem. Phys.* **1998**, *109*, 4758, and references therein.

(59) Li, G.; Hwang, H. J.; Jung, H. C. *Rev. Sci. Instrum.* **2005**, *76*, 023105 and references therein.

(60) Hess, W. P.; Kohler, S. J.; Haugen, H. K.; Leone, S. R. *J. Chem. Phys.* **1986**, *84*, 2143.

(61) Oberheide, J.; Wilhelms, P.; Zimmer, M. *Meas. Sci. Technol.* **1997**, *8*, 351.

(62) Parilis, E. S.; Kishinevskii, L. M. *Sov. Phys. Solid State* **1960**, *3*, 885.

(63) Krems, M.; Zirbel, J.; Thomason, M.; DuBois, R. D. *Rev. Sci. Instrum.* **2005**, *76*, 093305.

(64) Lias, S. G. Ionization Energy Evaluation In *NIST Chemistry WebBook, NIST Standard Reference Database Number 69*; Linstrom, P. J., Mallard, W. G. Eds.; National Institute of Standards and Technology: Gaithersburg, MD, 20899, 2005.

(65) Berkowitz, J.; Batson, C. H.; Goodman, G. L. *Phys. Rev. A* **1981**, *24*, 149.

(66) Robicheaux, F.; Greene, C. H. *Phys. Rev. A* **1992**, *46*, 3821.

(67) Wang, J., Yang, B., Cool, T. A., Hansen, N., Kasper, T. To be published.

(68) Berkowitz, J. *Photoabsorption, Photoionization, and Photoelectron Spectroscopy*; Academic: New York, 1979.

(69) Litorja, M.; Ruscic, B. *J. Chem. Phys.* **1997**, *107*, 9852.

(70) Chupka, W. A.; Lifshitz, C. *J. Chem. Phys.* **1968**, *48*, 1109.

JP8022937